Macromolecules

ARTICLE

pubs.acs.org/Macromolecules

Response to Shear Inversion of Polymer Brushes with Embedded Colloids

L. Spirin,[†,‡] A. Galuschko,[§,⊥] and T. Kreer*[,‡,§]

[†]Graduate School of Excellence "Material Science in Mainz", Mainz, Germany

[‡]Leibniz-Institut für Polymerforschung Dresden, Hohe Straße 6, 01069 Dresden, Germany

[§]Institut Charles Sadron, 23 rue du Loess, BP 84047, 67034 Strasbourg Cedex 2, France

[⊥]Institut für Theoretische Physik, Georg-August Universität, 37077 Göttingen, Germany

ABSTRACT: We present data from molecular dynamics simulations concerning the nonstationary response of polymer–brush bilayers to shear inversion. Bilayers with implicit solvents, dimeric solvents, and colloidal inclusions are subject to a quasi-instantaneous inversion of the shear direction, which mimics a highly nonstationary process. While we notice that the presence of an explicit solvent is essential to reproduce the experimentally observed mechanical instabilities, in particular an overshoot in the shear force, we also find that colloidal inclusions are capable of diminishing or even completely suppressing the instabilities. Our numerical data are complemented by scaling theory, where we determine a characteristic time scale that characterizes the response shortly after the inversion. In terms of chain length, N, shear rate, $\dot{\gamma}$, and distance between the grafting planes, D, we obtain $\tau \sim N/D\dot{\gamma}^{0.73}$ as the characteristic time, which is found to be in very good agreement with our numerical data. Our theory allows for predicting conformational and collective responses to shear inversion from static properties of the bilayer.

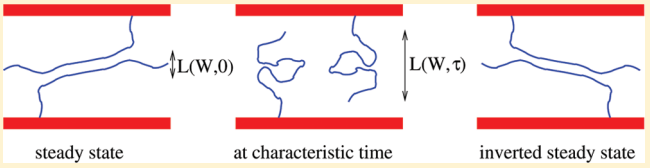

I. INTRODUCTION

Linear macromolecules can be grafted with one end onto a surface at such high densities that the individual chains repel each other strongly and stretch away from the surface forming a polymer brush.[1] Two brush-covered surfaces facing each other ("polymer-brush bilayer") can carry rather high loads and simultaneously reveal very small resistance to relative lateral motion.[2,3] Consequently, the resulting kinetic friction coefficient, defined as the ratio between friction force and normal load, can be orders of magnitude smaller than for dry friction,[2,3] i.e., in the absence of a lubricant. This motivated a large variety of experiments,[2−12] numerical studies,[13−37] and theoretical considerations.[33,37−43]

If nonlubricated, solid surfaces move relative to each other, their surface roughness or corrugation is responsible for large frictional losses. To a very large extent, these losses can be avoided by covering the surfaces with polymer brushes. Under strong shear, polymer-brush bilayers exhibit shear-thinning, i.e. a sublinear increase of the friction force with shear rate. This phenomenon, often observed for complex fluids (see, e.g., refs 44 and 45), is particularly pronounced for brushes, since the grafted layers can easily stretch and incline along the shear direction.[13] With this mechanism, the brushes reduce the width of their interpenetration, where dissipation takes place. Recent scaling arguments[33,34] seem capable of relating conformational and collective responses to steady (stationary) shear to the width of interpenetration. So far, the case of steady shear between polymer-brush covered surfaces appears to be well understood.

The situation is different for nonstationary shear, when the shear rate is time-dependent. Only few experimental[3,5,7,8] and numerical studies[19,25,37] were performed for such cases, covering oscillatory motion, relaxation from steady state toward static equilibrium or shear inversion, where the velocity of the sheared surfaces is (quasi-)instantaneously inverted. However, both in technical applications as in nature, nonstationary phenomena are much more common than steady-state motion.

In addition, biological systems, such as mammalian synovial joints, capillaries in plants or blood vessels, typically contain macromolecular inclusions. There are hardly any experiments[7] and only few numerical studies[28,30,31,34,35,37] known to us that focus on this aspect of polymer-brush lubrication.

In this article, we characterize the response of polymer-brush bilayers with (and without) colloidal inclusions to nonstationary shear using molecular dynamics simulations. In particular, we focus on conformational and collective properties of the bilayer when the direction of shear is inverted. Starting from a steady-state configuration, the inversion takes place on a time scale that is much smaller than the typical relaxation time of the bilayer. In this limit, the chains have not enough time to relax before they are fully exposed to the inverted shear field. This means that the shear inversion occurs quasi-instantaneously. In this way, we reproduce the response of a bilayer under large amplitude oscillatory shear (LAOS),[46] where the system reaches a steady state before the shear direction is inverted.

Received: June 27, 2011
Revised: October 28, 2011
Published: November 16, 2011

Complementing our numerical data, we present a scaling argument to determine a characteristic time, which is capable of describing the short time response of polymer-brush bilayers during the inversion of the shear direction. This concerns both conformational and collective properties of the bilayer. We compare systems at different shear velocities, far in the regime of nonlinear response, using bilayers with implicit solvents, explicit (dimeric) solvents, and various colloidal inclusions. Furthermore, we vary the molecular parameters of the brushes, i.e. density and length of the grafted chains.

In the next Section, we introduce the simulation method and parameters. Section III briefly revisits the stationary shear of polymer-brush bilayers with and without colloidal inclusions. In section IV we present our scaling approach and numerical data for the shear inversion. We first discuss conformational properties (section IV.A), before we turn to the collective response in shear direction (section IV.B). We then analyze density and velocity profiles in section IV.C. Section IV.D contains our results for the response in gradient direction. We finally present a short discussion of the influence of the "turn-time" (section IV. E) and conclude in section V.

II. SIMULATION METHOD

Our numerical approach is similar to those in refs 14, 18, 22, 23, 25, 26, 28−30, 33, 34, and 37. We use the Kremer−Grest (KG) model,[47] which is a generic coarse-grained model for polymer chains. Here, monomers are represented as Lennard-Jones (LJ) spheres, interacting via a truncated and shifted potential,

$$U_{\mathrm{LJ}}(r_{ij}) = 4\varepsilon[(\sigma/r_{ij})^{12} - (\sigma/r_{ij})^{6} - (\sigma/r_c)^{12} + (\sigma/r_c)^{6}] \quad (1)$$

The units of energy and length are defined by ε and σ, respectively. r_{ij} denotes the distance between monomer i and j and r_c is the cutoff radius. We consider a purely repulsive potential, i.e. we choose $r_c = 2^{1/6}\sigma$, and shift U_{LJ} to avoid a discontinuous force at the cutoff. The connectivity along the chain backbone is given by the FENE potential,[47]

$$U_{\mathrm{FENE}}(r) = -\frac{1}{2} k r_0^{\,2} \ln[1 - (r/r_0)^2] \quad (r < r_0) \quad (2)$$

where r is the distance between neighboring monomers in a chain, $k = 30\varepsilon/\sigma^2$, and $r_0 = 1.5\sigma$ the maximum allowed bond length.

The polymers are grafted onto surfaces with one end. As substrates we use rigid, two-dimensional hexagonal lattices with surface area $A = L_x L_y = 42\sigma \times 36.373\sigma = 1527.666\sigma^2$, where L_x and L_y are the extensions of a substrate in shear and neutral direction, respectively (see Figure 1).

Our simulated chains each consist of $N = 30$ or $N = 60$ monomers. The latter value of N should already exhibit indications of reptation dynamics in the bulk. However, ref 48 suggests that the entanglement length increases with decreasing thickness of a confined concentrated solution. Moreover, the entanglement length should be larger for directed chains in a polymer brush than in the bulk. Our recent study[34] of polymer-brush bilayers indeed reveals no influence of entanglements for $N = 120$ at stationary shear.

The surface density of grafted chains is varied from $\rho_g \approx 2.2\rho_g^*$ to $\rho_g \approx 4.4\rho_g^*$, where $\rho_g^* = 1/\pi R_g^{\,2}$ refers to the surface density at which chains of $N = 30$ start to overlap.[49] The value of ρ_g^* follows from the mean square radius of gyration

$$R_g^{\,2} \equiv \langle R_g^{\,2} \rangle \equiv \frac{1}{N} \langle \sum_i (r_i - r_{\mathrm{cm}})^2 \rangle \quad (3)$$

of isolated chains in solution,[50] where r_{cm} is the chain's center-of-mass position vector, r_i is the monomer position, and the average is taken over all simulated chains. We choose the grafting sites randomly and allow the grafted ends to find their (local) equilibrium positions on the substrates before shear is applied. During shear, we verify that the grafted ends do not slip along the substrate but remain at their original positions.

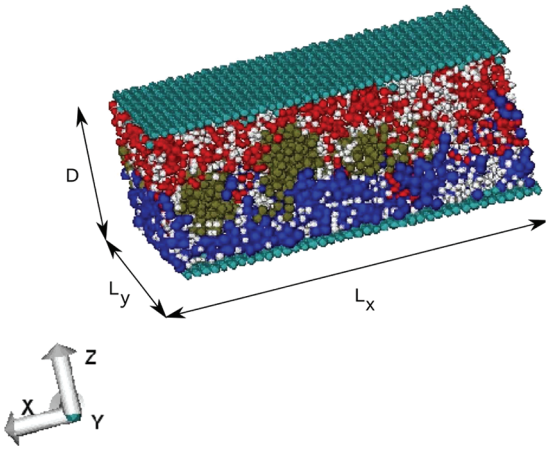

Figure 1. Snapshot of a simulated system (C1) with colloidal inclusions (green spheres) at large constant shear. The polymer brushes (blue and red) are grafted to atomically smooth surfaces (dark gray). Solvent dimers are represented as light gray spheres.

All monomers (polymers, solvent, and colloids) interact with the wall atoms via eq 1. Here, we use the same values for r_c, σ, and ε as for the monomer−monomer interaction. Only for interactions between the grafted end-monomers and the wall atoms we increase ε by a factor of 100 with respect to the monomer−monomer interaction and make the LJ potential attractive by doubling r_c. The wall atoms remain at their ideal lattice positions relative to each others and move only with the given shear velocity. Parallel to the surfaces, periodic boundary conditions are implemented.

We introduce LJ dimers as solvent molecules. Our main motivation for using dimers is to avoid packing effects, which are more likely to occur for single monomers. The dimers are connected via eq 2 with the same interaction parameters as for the monomer−monomer interaction. Consequently, the Flory−Huggins parameter, χ, vanishes and hence the excluded volume parameter, $v \approx a^3(1 - 2\chi) \approx a^3$ (a the effective monomer size), is always positive, independent of the temperature,[51] leading to athermal (good) solvent conditions.

Apart from this simple solvent, we include colloids of varying softness. The colloids are represented by star-polymers with different functionalities, $f = 10$, 30, and arm lengths, $m = 5$, 15. We cover the colloidal limit of almost hard spheres, with large values of f and short arms, up to very fluffy stars, with small number of arms and large values of m. The different model solvents considered in this article are the following: Solvent A is an implicit solvent, where no dimers or colloids are incorporated. Solvent B represents the dimeric solvent, and solvent C1 is a mixture of dimers and stars with $f = 30$ arms and $m = 5$ monomers

Table 1. Composition for Different Solvent Types and Prefactor α [eq 29] to Obtain a Maximum for $N_{int}(t)$ at $t/\tau' = 1$ (See Section IV.A, Figure 7)

solvent	% dimers	% colloids	α
A	-	-	0.57
B	100	-	1.01
C1	50	50, $f = 30$, $m = 5$	1.08
C2	50	50, $f = 10$, $m = 15$	1.17
D1	-	100, $f = 30$, $m = 5$	1.44
D2	-	100, $f = 10$, $m = 15$	1.62

in each arm. Each arm is connected to one central monomer. Softer stars are introduced with $f = 10$ and $m = 15$ (solvent C2). Compared to solvent B, (approximately) half of the dimers are replaced by colloids. For the solvents D1 and D2 we use the stars corresponding to C1 and C2, respectively, but now we replace all dimers by colloids. The total monomer number density (brushes, dimers, and stars) is for all cases, except for solvent A, $\rho = 0.9$. The different compositions for the solvents used in this article are compiled in Table 1.

We solve Newton's equations of motion with the velocity–Verlet algorithm[52] using a time-step of $\Delta t = 2 \cdot 10^{-3}\tau_{LJ}$ [$\tau_{LJ} = \sigma(m_p/\varepsilon)^{1/2}$ the LJ time unit]. The particle mass, m_p, is set to unity for all monomers of polymer chains, dimers, and colloids.

Using a dissipative particle dynamics (DPD) thermostat[52−56] temperature is kept constant at $T = 1.68\varepsilon/k_B$ (k_B the Boltzmann constant). The thermostat adds to the conservative force a dissipative force, F_i^D, and a random force, F_i^R. Both forces are applied in a pairwise form, such that the sum of thermostatting forces acting on a particle pair vanishes. With Γ the friction constant, the dissipative force reads

$$\mathbf{F}_i^D = -\Gamma \sum_{j(\neq i)} \omega^D(r_{ij})(\hat{\mathbf{r}}_{ij} \cdot \mathbf{v}_{ij})\hat{\mathbf{r}}_{ij} \quad (4)$$

where $\hat{\mathbf{r}}_{ij} = (\mathbf{r}_i - \mathbf{r}_j)/r_{ij}$ and $\mathbf{v}_{ij} = \mathbf{v}_i - \mathbf{v}_j$. We use the commonly employed weight function

$$\omega^D(r_{ij}) = \begin{cases} (1 - r_{ij}/r_c)^2 & (r_{ij} < r_c) \\ 0 & (r_{ij} \geq r_c) \end{cases} \quad (5)$$

with the same cutoff range r_c as for the LJ interaction. The random force is given by

$$F_i^R = \lambda \sum_{j(\neq i)} \omega^R(r_{ij})\theta_{ij}\hat{\mathbf{r}}_{ij} \quad (6)$$

where θ_{ij} represents a random variable with zero mean, unit variance, and $\theta_{ij} = \theta_{ji}$. The weight function for the random force is $\omega^R(r_{ij})$. Friction and noise strength, λ, define the temperature via $\lambda^2 = 2k_BT\Gamma$. As previously, we choose $\Gamma = 5\tau_{LJ}^{-1}$, which appears to be a good compromise between stability and accuracy.[33]

To fulfill the fluctuation–dissipation theorem the weight functions for dissipative and random forces have to satisfy the relation

$$[\omega^R]^2 = \omega^D \quad (7)$$

Alternative weight functions have been tested previously.[29]

During shear, we keep the distance between the surfaces, D', constant. In the following, we characterize the compression of the bilayer by the (mean) distance between the grafting planes, $D = D' - 2r_c = D' - 2 \times 2^{1/6}\sigma$. We consider only one degree of compression, $D = 17.5\sigma$. This value is small enough to ensure an almost flat monomer density profile of the brushes, whereas it is large enough that the system can contain a reasonable amount of dimeric solvent and colloids. Figure 1 shows a typical snapshot obtained from our simulations at large constant shear.

Shear inversion is performed by transferring the velocity of a substrate, v, at steady state to its negative value in a gradual manner, such that the resulting accelerations remain finite. The time window, in which the inversion is performed, is small compared to the relaxation time of the bilayer (see section III). Therefore, the grafted layers cannot relax before the substrates reach their new (inverted) velocity and the inversion process is thus highly nonstationary. Since we start out from a well established steady-state configuration, we reproduce the inversion during LAOS experiments.

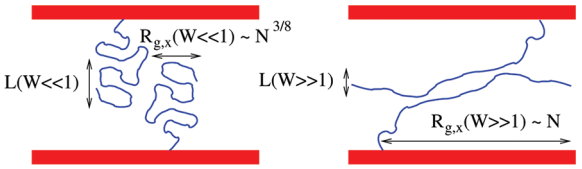

Figure 2. Sketch of grafted polymer chains belonging to upper and lower brushes at small shear rate ($W \ll 1$, left) and at large shear rate ($W \gg 1$, right). For $W \ll 1$, the lateral chain extension is unperturbed, such that $R_{g,x}(W \ll 1) \sim N^{\nu/2(3\nu-1)} \approx N^{3/8}$, whereas at very large shear $R_{g,x}(W \gg 1) \sim N$. The interpenetration length, $L(W)$, is reduced at large shear compared to its value in the linear response regime.

III. SCALING THEORY FOR STEADY SHEAR, REVISITED

In this section, we review the theoretical predictions for polymer-brush bilayers under steady shear, as they have been proposed originally in ref 33. The central idea of a self-regulating interpenetration thickness has been anticipated even earlier.[2,3,5] We first consider the regime of linear response (small shear rates), before we turn to the phenomenon of shear thinning. As already mentioned in the previous section, we can neglect entanglements and related effects, as for instance the "arm-retraction" mechanism,[3] for the chain lengths considered here.

A. Linear Response Regime. With the parameters introduced above, we simulate semidilute brushes in the regime of strong compression,[33,34] which means that the total monomer density profile (sum of both brush profiles) is flat throughout the gap, apart from typical oscillations close to the substrates. Therefore, the size of concentration blobs, ξ, is constant, at least in the region, where the two brushes overlap. The monomer concentration is given by $c = 2N\rho_g/D$ and because of $\xi \sim a(ca^3)^{\nu/(1-3\nu)}$,[57] one finds

$$\xi \sim a\left(a^3 \frac{N\rho_g}{D}\right)^{\nu/(1-3\nu)} \quad (8)$$

with $\nu \approx 0.588$ the Flory exponent.

The dissipation in a sheared polymer-brush bilayer occurs within the interpenetration zone between the two brushes. For brushes at melt density, the width of interpenetration reads[33]

$$L \sim \left(\frac{N^2a^4}{D}\right)^{1/3} \quad (9)$$

dx.doi.org/10.1021/ma2014029 |Macromolecules 2011, 44, 9399–9410

This equation holds for a semidilute bilayer, which can be regarded as a dense melt of concentration blobs of size ξ, with the replacements[57]

$$N \rightarrow \frac{N}{g} \quad \text{and} \quad a \rightarrow \xi \tag{10}$$

Here, $g = (\xi/a)^{1/\nu}$ denotes the number of monomers within a blob. Using this transformation together with eq 8, one arrives at an interpenetration length of

$$L \sim a\left[N^{2\nu}(\rho_g a^2)^{2(1-2\nu)}\left(\frac{a}{D}\right)^{1-\nu}\right]^{1/(3\nu-1)} \tag{11}$$

for strongly compressed, semidilute brushes.

Similar considerations can be made for the extension of a grafted chain parallel to the surfaces, $R_{g,x}(0)$, with x the direction of shear. Under melt conditions, the zero-shear chain extension reads $R_{g,x}(0) = N^{1/2}a$. Using the transformation (10) together with eq 8 yields

$$R_{g,x}(0) \sim a\left[N^{\nu}\left(\frac{D}{\rho_g a^3}\right)^{2\nu-1}\right]^{1/2(3\nu-1)} \tag{12}$$

for the lateral chain extension of semidilute brushes. For small shear rates, $\dot\gamma \equiv 2\nu/D$, the conformation of the chains should not depend on $\dot\gamma$. Therefore, we expect $R_{g,x}(\dot\gamma) = R_{g,x}(0)$ in the regime of linear response.

In the same limit, the shear force is proportional to the shear rate. Here, the friction force per unit area (f_x/A) can be estimated by assuming Zimm dynamics in the blob. There are $cL(a/\xi)^{1/\nu}$ blobs per unit area in the interpenetration zone. For each blob, we have a friction coefficient of $\eta_s\xi$, with η_s the solvent viscosity. For a shear rate of $\dot\gamma$, the typical velocity is $\dot\gamma D$. Thus, we may write

$$\frac{f_x(\dot\gamma)}{A} \sim cL\xi^{(\nu-1)/\nu}a^{1/\nu}\eta_s\dot\gamma D \tag{13}$$

and, with eqs 8, 11, and 13, we find

$$\frac{f_x(\dot\gamma)}{A} \sim \left[N^{8\nu}(\rho_g a^2)^{2(1+\nu)}\left(\frac{a}{D}\right)^{4(1-\nu)}\right]^{1/(3\nu-1)}\eta_s\dot\gamma \tag{14}$$

for the shear force in the regime of linear response.

To characterize the strength of shear, one typically compares the shear rate to the largest relaxation time of the bilayer, τ_b, by defining the Weissenberg number, $W \equiv \dot\gamma\tau_b$. It can be shown[33] that τ_b corresponds to the relaxation time of a single chain within the brush, which might seem surprising. However, this relation follows (by pure coincidence) if one accounts for thermal fluctuations that allow the chain to exchange between the overlap region and deeper layers of the brush, such that the shear stress is sustained by more chains than only those in the interpentration layer. A detailed analysis is given in the Appendix of ref 33. For melt conditions one may write $\tau_b = N^2\tau_0$, with τ_0 the time for a monomer to diffuse over its own size. Renormalizing to concentration blobs yields

$$\tau_b \sim N^2\left(\frac{a}{\xi}\right)^{2/\nu}\tau_\xi \tag{15}$$

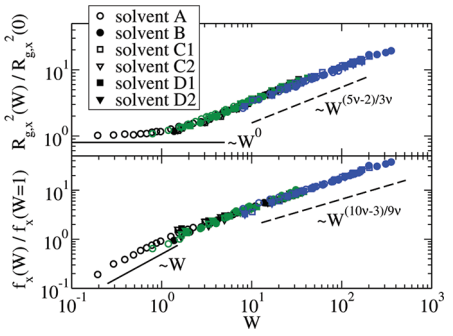

Figure 3. Mean square radius of gyration divided by its value at static equilibrium (above) and rescaled shear force (below) versus Weissenberg number for different solvents (see text). Key: black, $N = 30$, $\rho_g/\rho_g^* \approx 2.2$; green, $N = 30$, $\rho_g/\rho_g^* \approx 4.4$; blue, $N = 60$, $\rho_g/\rho_g^* \approx 2.2$.

thus, with $\tau_\xi \sim (\xi/a)^3\eta_s a^3/k_BT$, the Zimm relaxation time of a blob, we find [using eq 8]

$$\tau_b \sim \frac{\eta_s a^3}{k_BT}\left[N^{3\nu}\left(\frac{\rho_g a^3}{D}\right)^{2-3\nu}\right]^{1/(3\nu-1)} \tag{16}$$

The regime of linear response is left when the external driving force exceeds the typical strength of thermal fluctuations, such that the bilayer cannot relax fast enough to maintain its equilibrium conformation. The crossover from linear response to shear thinning should thus occur at $W = 1$, i.e., at a shear rate that corresponds to the inverse relaxation time of the bilayer. With eqs 14 and 16 we obtain the force at which the system leaves the linear response regime,

$$\frac{f_x(W=1)}{A} \sim \frac{k_BT}{a^3}\left[N^{-\nu}(\rho_g a^2)^{11\nu-4}\left(\frac{a}{D}\right)^{5\nu-2}\right]^{1/(3\nu-1)} \tag{17}$$

B. Shear Thinning Regime. For large shear rates ($W \gg 1$), the chains stretch and incline along the shear direction. The limiting case is reached when the chains are fully stretched, i.e. $R(W \gg 1) \sim N$ (see Figure 2). Equation 16 suggests $W \sim N^{3\nu/(3\nu-1)}$ and from eq 12 we obtain

$$\frac{R_{g,x}(W \gg 1)}{R_{g,x}(0)} \sim N^{(5\nu-2)/2(3\nu-1)} \sim W^{(5\nu-2)/6\nu} \tag{18}$$

or, with $\nu \approx 0.588$, $R_{g,x}(W \gg 1)/R_{g,x}(0) \sim W^{0.27}$.

In a similar way we can predict the dependence of the shear force on W for large shear rates. For strongly stretched chains, every monomer is exposed to the shear flow, thus $f_x(W \gg 1) \sim N$. Equation 17 leads to

$$\frac{f_x(W \gg 1)}{f_x(W=1)} \sim N^{(10\nu-3)/3(3\nu-1)} \sim W^{(10\nu-3)/9\nu} \tag{19}$$

or, $f_x(W \gg 1)/f_x(W = 1) \sim W^{0.54}$ ($\nu \approx 0.588$).

Both power laws [eqs 18 and 19] are put to a test in Figure 3. We observe a universal behavior, which is reproduced independently of the considered solvent. Even systems with colloidal inclusions exhibit the predicted response. This may indicate that the colloidal inclusions, at least for the considered parameter combinations of f and m, relax much faster than the brushes,

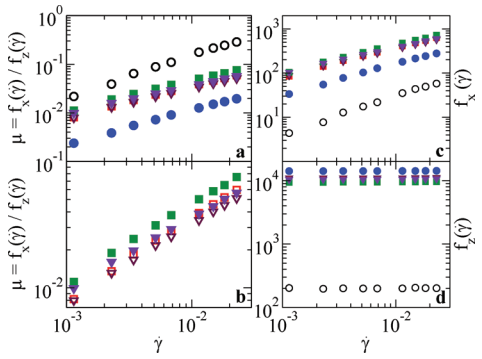

Figure 4. Kinetic friction coefficient for bilayers with $N = 30$ and $\rho_g/\rho_g^* \approx 2.2$ as a function of shear rate for all solvents (a, same legend as in Figure 3) and for colloidal inclusions only (b). The right side shows shear force (c) and normal force (d).

which thus dominate the response to shear. In fact, as we will see below (section IV. C), the stars hardly translate but rather rotate during shear. Note that system A remains the longest in the linear response regime, while the colloidal inclusions (C1−D2) drive the system into the non-Newtonian regime faster than the simple (dimeric) solvent B. A detailed comparison between the responses of the bilayer without (A) and with explicit solvent (B) can be found in ref 33.

An important feature divulges when we compare the kinetic friction coefficient, μ, which is defined as the ratio between shear and normal forces, $f_z(W)$, for the different investigated systems (Figure 4a).[58] Interestingly, we find the smallest value of μ for solvent B and the largest for solvent A, while systems with colloidal inclusions are found somewhere between these two cases. Two conclusions may be drawn from this. First, the presence of an explicit solvent lowers the friction coefficient as compared to the implicit solvent, highlighting the importance of solvent for the lubrication properties of the bilayer. The second conclusion, namely that colloidal inclusions increase μ as compared to system B, may come as a surprise. As the right side of Figure 4 shows, colloidal systems (C1−D2) lead to an increased friction coefficient because they invoke a larger friction force (c), due to their overlap with the brushes, and simultaneously they show a smaller normal force (d). The reduction of f_z, as compared to the dimeric solvent, stems from the additional connectivity within polymer stars, which leads to a smaller excluded volume per monomer (keeping in mind that we keep the overall monomer density constant).

As Figure 4b shows, we observe a larger value of μ for systems with larger density of inclusions. The reason is obvious, as the effects described in the previous paragraph are enhanced when the density of the inclusions is increased. Comparing systems of hard inclusions (C1, D1) to the corresponding systems with soft inclusions (C2, D2) reveals a smaller kinetic friction coefficient for the softer colloids. It seems that the latter can deform more easily, such that they offer less resistance to shear.

However, it may be surprising that colloidal inclusions increase μ, because macromolecular inclusions are very often present in biological systems. It appears counterintuitive that nature, after a long evolutionary process, does not find the optimal solution to prevent frictional loss or wear. Below, we demonstrate that there is a distinct advantage of colloidal (or, in general, macromolecular) inclusions, which is related to the mechanical stability during nonstationary processes, providing a possible explanation why biological systems contain macromolecular inclusions.

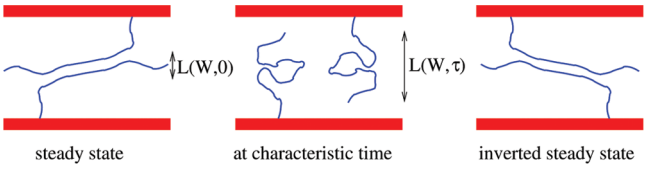

Figure 5. Sketch of grafted polymer chains belonging to upper and lower brushes at steady state ($W \gg 1$), during shear inversion at the characteristic time $t = \tau$ (see text), and in the inverted steady state configuration. Since the chains have to invert their orientation, the interpenetration length, L, undergoes a maximum at $t = \tau$.

Before turning our attention to the case of shear inversion, we want to emphasize that the semidilute limit of asymptotically large (dilute) blobs is far from being reached in the simulation. Nonetheless, it is well documented that simulation data with amazingly small blobs do follow the semidilute picture for both statics and dynamics.[59] The reason is that the "Des Cloizeaux" picture[60] was developed in the weak coupling limit, where small blobs are not swollen. In marked contrast, the simulations start out from a bare coupling (interaction) larger than the asymptotic value (fixed point) and thus belong to the strong coupling regime.[61] In the simulation, small chain sections are actually (slightly) overswollen. This also explains the success of simulations to measure values of the swelling exponent from short chains.

IV. RESPONSE TO SHEAR INVERSION

We now turn to the shear inversion. Our starting point is a bilayer at steady shear, where the substrates are at constant velocity, v and $-v$, respectively. We invert the direction of shear by exchanging the signs of the velocities. This is not done abruptly, which would provoke infinite accelerations, but on a finite time scale that is small compared to the largest relaxation time of the bilayer [eq 16]. To this extend, we use the velocity protocol

$$v(t) = \begin{cases} v & (t \le t_0) \\ v \cos \dfrac{\pi(t - t_0)}{\tau_i} & (t_0 \le t \le t_0 + \tau_i) \\ -v & (t \ge t_0 + \tau_i) \end{cases} \qquad (20)$$

with t_0 the time of inversion and $\tau_i \ll \tau_b$ the time window, in which the inversion takes place ("turn-time"). For the following presentation of our data, we shift the time axis such that $t_0 = 0$. The steady state, from which we start the inversion, then takes place at negative values on the time axis.

A. Conformational Response. At large steady shear, the chains are strongly stretched along the direction of shear. When the shear direction is inverted, the chains have to change their conformation such that they stretch in the opposite direction. Hence, the bilayer must undergo a time window, in which the chains (in average) are oriented orthogonal to the substrates (see Figure 5). Thus, the interpenetration width of the bilayer must exhibit a maximum. Unfortunately, it is very difficult to monitor the interpenetration width [eq 11] directly in the simulation. Instead, we characterize the amount of interpenetration between

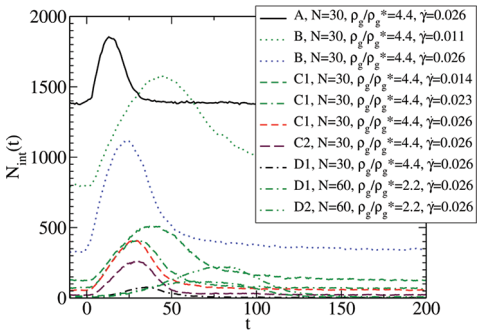

Figure 6. Number of binary interbrush contacts per unit time during shear inversion at $t_0 = 0$.

the brushes by counting the number of binary interbrush contacts per unit time, N_{int}.[23] Previous investigations[23,25,28,33,37] have shown a strong correlation between N_{int} and the response of the bilayer both to stationary and nonstationary shear.

Figure 6 shows N_{int} as a function of time during shear inversion. Note that we find the largest overlap for the implicit solvent, whereas colloidal inclusions lower N_{int} drastically.

The appearance of a maximum in N_{int} allows to define a characteristic time for the inversion process (see Figure 5). The latter may be calculated using a simple scaling argument: When starting from a steady-state configuration at large shear ($W \gg 1$) and inverting the direction of shear, the chains have no time to relax significantly before the grafted chain end has moved below the free end. Therefore, the time-development of the chain extension for short time scales may be written as

$$\frac{R_{g,x}(W,t)}{R_{g,x}(W)} = 1 - \frac{t\dot{\gamma}D}{2R_{g,x}(W)} \tag{21}$$

where $R_{g,x}(W)$ is the steady-state radius of gyration in shear direction and $R_{g,x}(W,t)$ its time-dependent value. This implies that a minimum in $R_{g,x}(W,t)$ occurs at a characteristic time

$$\tau \sim \frac{R_{g,x}(W)}{\dot{\gamma}\, D} \tag{22}$$

Using eq 18 we thus may write

$$\tau \sim \frac{R_{g,x}(0)}{D}\,[\dot{\gamma}^{-(\nu+2)}\tau_b^{(5\nu-2)}]^{1/6\nu} \tag{23}$$

or, with $\nu \approx 0.588$

$$\tau \sim \frac{R_{g,x}(0)}{D}\,\dot{\gamma}^{-0.73}\tau_b^{0.27} \tag{24}$$

Equation 23 also can be derived using a somewhat different argument. For large shear rates, we may imply that τ is related to a length scale that scales linearly with N, such that we may assume $\dot{\gamma}\tau \sim N$. On the other hand, we can write

$$\dot{\gamma}\tau \sim \frac{R_{g,x}(0)}{D}\,\tilde{g}(\dot{\gamma}\tau_b) \tag{25}$$

with $\tilde{g}(\dot{\gamma}\tau_b) \sim (\dot{\gamma}\tau_b)^p$ a scaling function. Using eqs 12 and 16, we obtain

$$\dot{\gamma}\tau \sim N^{\nu/2(3\nu-1)}[\dot{\gamma}N^{3\nu/(3\nu-1)}]^p \sim N \tag{26}$$

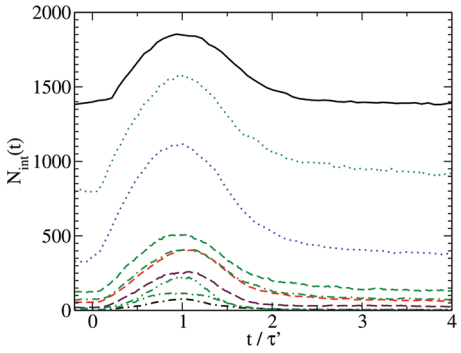

Figure 7. Number of binary interbrush interactions as a function of rescaled time, using eq 29 with the prefactors of Table 1. Same legend as in Figure 6.

which leads to $p = (5\nu - 2)/6\nu$, yielding the same expression for τ as given in eq 23. This consistency provides an additional confirmation of our underlying approach for steady-state shear.

To express τ in terms of the molecular parameters, we replace $R_{g,x}(0)$ and τ_b in eq 23 respectively by eqs 12 and 16, which yields

$$\tau \sim \frac{N}{D}\left(\frac{D}{\rho_g}\right)^{(21\nu - 19 + 4/\nu)/6(3\nu-1)} \dot{\gamma}^{-(\nu+2)/6\nu} \tag{27}$$

where we have set a, η_s, and k_BT to unity. Using again $\nu \approx 0.588$, we obtain

$$\tau \sim \frac{N}{D^{0.97}\rho_g{}^{0.03}\dot{\gamma}^{0.73}} \approx \frac{N}{D\dot{\gamma}^{0.73}} \tag{28}$$

which implies virtually no dependence of τ on the grafting density.

We may test our prediction for the characteristic time by plotting N_{int} as a function of a rescaled time, as done in Figure 7. To obtain the maximum at unity we introduce a prefactor in eq 28, i.e., we write

$$\tau' = \alpha\frac{N}{D\dot{\gamma}^{0.73}} \tag{29}$$

and plot the data against t/τ'. The prefactor α is constant for a given model solvent when N, ρ_g, or $\dot{\gamma}$ are varied, but differs when different solvent types are compared (see Table 1). The reason is obvious, as the parameters a and η_s, which enter as prefactors in eq 28, depend on the composition of the considered system.[62]

Similarly, we may test our approach using the chain extension in shear direction. Figure 8 shows the ratio $R_{g,x}(W,t)/R_{g,x}(W)$ as a function of rescaled time, where we have used eq 29 as the characteristic time. It turns out that this pathway is not very successful, as we do not obtain a universal behavior. In fact, enforcing that all maxima in Figure 7 align leads to a misleading picture. We will see below that not all systems follow the simple picture precisely, because sometimes the relaxation of the chains sets in before the maximum in N_{int} is reached, while other systems are not far enough in the regime of nonlinear response. However, when using eq 23, where the prefactors a and η_s are intrinsically included in $R_{g,x}(0)$ and τ_b, we find that the short-time response of our brushes to shear inversion is well described by the proposed model (see Figure 9). Here and in the following, we used a constant prefactor of approximately 100 independently of the considered system.

dx.doi.org/10.1021/ma2014029 |Macromolecules 2011, 44, 9399–9410

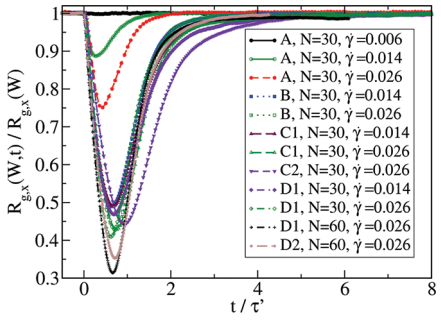

Figure 8. Radius of gyration in shear direction normalized by its steady-state value as a function of rescaled time, using eq 29 with the prefactors of Table 1. The reduced grafting density is $\rho_g/\rho_g^* \approx 2.2$ for all systems.

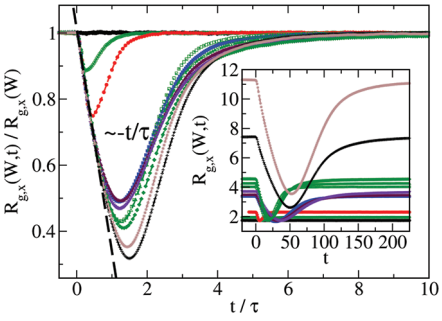

Figure 9. Same data as in Figure 8, now using eq 23 as the characteristic time, τ. The inset shows the unscaled data.

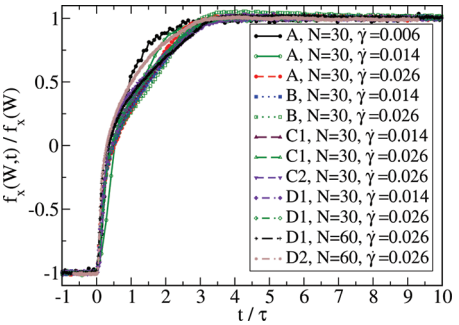

Figure 10. Shear force normalized by its steady-state value as a function of rescaled time [τ from eq 23]. The reduced grafting density is $\rho_g/\rho_g^* \approx 2.2$ for all systems.

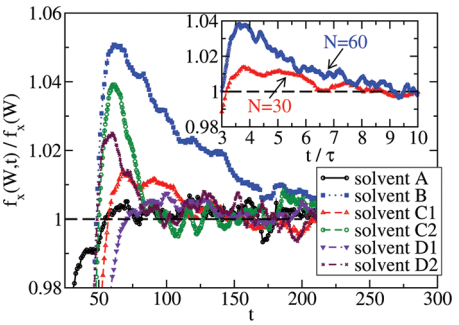

Figure 11. Time-development of the shear force for $N = 30$, $\rho_g/\rho_g^* \approx 4.4$, $\dot{\gamma} = 0.026$. We observe an overshoot for the dimeric solvent (B), which is not reproduced by the implicit solvent (A). Systems with colloidal inclusions (C1−D2) show a reduced overshoot. For the system with hard colloids at the larger density (D1), the overshoot is completely suppressed. Inset: Overshoot for the two considered chain lengths (solvent C1) on rescaled time axis.

The data belonging to solvent A do not follow the general trend. While for all other solvents, after a linear decrease of $R_{g,x}$, the minimum appears at approximately the same value of t/τ, solvent A leaves the universal linear decrease and reveals its minimum much earlier. For the smallest considered shear rate, we observe no response at all. The reason for this behavior may be that the systems with solvent A are not far enough inside the nonlinear regime, such that the simple model (stretched chains that have no time to relax) does not describe even the short-time behavior.

For larger times, $t > \tau$, we observe a slow increase of $R_{g,x}$ toward the new steady state. Here, two effects mix; on one hand, the grafted end now moves away from the free chain end, but simultaneously the chain tends to relax. From an analytical point of view, the interference of the relaxation process with our simple approach is difficult to describe and there appears to be no straightforward way to present a universal scaling plot for the response of the bilayer on time scales beyond τ.

B. Collective Response in Shear Direction. We now use the same approach to analyze the collective response of the bilayer in shear direction. Figure 10 displays the time-development of the shear force, $f_x(W,t)$, normalized by its steady-state value, $f_x(W)$, as a function of rescaled time, t/τ. We observe that almost all models with explicit solvent can be superimposed onto a master curve, even for intermediate and large time scales, where our simple scaling argument should not be applicable. Exceptions are given by the purely dimeric solvent, where we observe an overshoot (see below), and the system D2 with $N = 60$. Though the latter system follows our predictions for steady-state shear, it cannot be described perfectly by our simple approach for shear inversion on intermediate time scales. As it seems, the relaxation of the longer, grafted chains and possible inertia effects invoked by the fluffy stars at large density become important for system D2. Presumably for the same reason as above, solvent A clearly deviates from the general picture, partially even on short time scales.

When comparing shear force and chain extension (Figure 9), we observe that the collective quantity reaches the inverted steady state sooner than $R_{g,x}$. As it seems, the chains first need to feel a time-independent force before the chain extension can become stationary (albeit from fluctuations).

Interestingly, when zooming into the region where the shear force has just reached its new steady-state value, as done in Figure 11, we observe an overshoot for some system parameters. While the dimeric solvent exhibits this overshoot clearly, the implicit solvent fails to display the effect. Two possible explanations can be given: First, it may be that the incompressibility, which is not present for the implicit solvent, is needed to reveal the overshoot, as for solvent A the chains have the chance to reduce the overlap by simply shrinking without a penalty for the solvent that has to be squeezed into the overlap region. A second reason again may be that the system is not far enough inside the nonlinear regime.

The occurrence of an overshoot is in agreement with experiments[7,8] that have been performed (almost) in the LAOS regime. It is rather unfavorable, as it may lead to additional wear, e.g., during oscillatory motion. However, our data indicate that

dx.doi.org/10.1021/ma2014029 |*Macromolecules* 2011, 44, 9399–9410

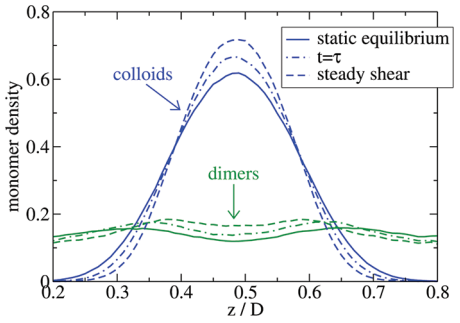

Figure 12. Density profiles of dimers and monomers of colloidal inclusions (system C1) at static equilibrium, in steady state, and during the inversion, approximately when the number of binary interbrush interactions exhibit a maximum (see Figure 7). The chain length is N = 30, $\rho_g/\rho_g^* \approx 4.4$, and $\dot{\gamma} = 0.026$.

the overshoot can be drastically reduced (solvents C1, C2, D2) or even be completely suppressed (solvent D1) when colloidal inclusions are embedded inside the bilayer. This seems to solve our puzzle, namely why biological systems often contain such inclusions. Despite that macromolecules increase the kinetic friction coefficient during steady-state shear, they prevent the bilayer from mechanical instabilities during shear inversion or comparable nonstationary processes. Apart from biological systems, this mechanism may be useful in technical applications.

The physical explanation for the ability of macromolecular inclusions to reduce the overshoot should be related to the strong correlation between the overlap and the shear force. Essentially, the overshoot results from the increase of N_{int} during the inversion. As can be seen from Figures 6 and 7, the number of binary interbrush interactions is significantly smaller for systems with inclusions than for the dimeric solvent, as the inclusions hamper the interpenetration. In addition, the colloids cannot deform significantly during shear, even when the shear direction is inverted. Consequently, the overshoot must be smaller for these systems.

We anticipate that the overshoot exceeds the steady-state value only by a few percent, such that one might argue that the effect is rather small and hence not important for any practical purposes. However, in the inset of Figure 11 we show, for the example of system C1, that the overshoot increases strongly with N. This explains why the effect is much more pronounced in experimental systems,[8] where the chain length is at least 1 to 2 orders of magnitude larger than in our simulations.

Before discussing the collective response in gradient direction, we first focus on density and velocity profiles of the confined liquid. The latter appear to be essential for understanding the response of the normal force to shear inversion.

C. Density and Velocity Profiles During Shear Inversion. When a polymer-brush bilayer is subject to large steady shear and the chains incline in shear direction, the brushes densify and reduce their overlap.[23] This means that part of the solvent is squeezed into the overlap region.[33] When the shear direction is inverted and the overlap between the brushes increases again within a certain time window, the solvent flows back into the brushes. Figure 12 clearly displays this behavior for system C1, revealing that more solvent dimers accumulate in the center of the bilayer during steady state as compared to static equilibrium, while part of the solvent has flown back during the inversion at $t \approx \tau$. Similar conclusions can be drawn for the monomers of the

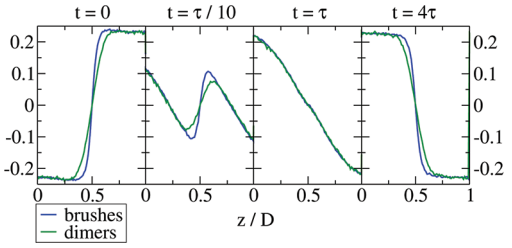

Figure 13. Velocity profiles for monomers of brushes and dimers at steady state (t = 0), shortly after the inversion ($t \approx \tau/10$), at the characteristic time ($t \approx \tau$), and close to the inverted steady state ($t \approx 4\tau$) for system B with N = 30, $\rho_g/\rho_g^* \approx 2.2$, $\dot{\gamma} = 0.026$.

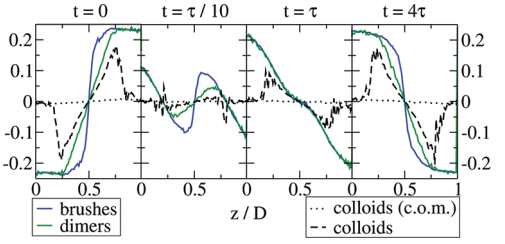

Figure 14. Same data as in Figure 13, now for system C1. While the centers-of-mass (c.o.m.) of the colloids are almost at rest, we observe a rotational motion of their monomers.

colloidal inclusions. The backflow of dimers is significantly weaker than for system B (see ref 33), because the colloids occupy most of the space between the brushes. As already mentioned, the colloids hardly deform under shear.

We now turn to the velocity profiles of the dimeric solvent, the colloids, and the brushes for the systems B (Figure 13) and C1 (Figure 14). For system B, the dimeric solvent in the overlap region reveals an almost linear velocity profile at steady state (t = 0), as to be expected for a Newtonian solvent. On the other hand, the velocity profile for the brushes is nonlinear. Around the interpenetration zone, the velocity is even larger than the applied shear velocity. This behavior may result from a cyclic motion of the chain ends, which is discussed in detail elsewhere.[20,31,43]

Shortly after the inversion ($t \approx \tau/10$), the velocity profiles of both solvent and brushes are strongly distorted. At $t \approx \tau$, i.e., approximately when the binary interactions between the brushes reach their maximum, the velocity profiles of brushes and solvent cannot be distinguished. The layers close to the substrates have already adopted the new shear velocity, and, more importantly, both profiles, even that of the brushes, are linear. This indicates that the grafted chains loose the information about their connectivity, behaving like an ordinary Newtonian solvent. The new, stationary velocity profile is found at $t \approx 4\tau$, though the cyclic motion has not established so far.

Figure 14 displays the velocity profiles for system C1. We observe almost the same properties for the profiles of brushes and dimeric solvent as for system B. The centers-of-mass of the colloidal inclusions remain almost at rest, both in steady state and during inversion. However, the monomers belonging to the colloids clearly display nonvanishing velocities, indicating hence a rotational motion of the inclusions.

Immediately after the inversion ($t \approx \tau/10$), when the profiles of brushes and dimeric solvent display very similar features as for system B, the colloids rotate slower. Their velocity profile reveals

dx.doi.org/10.1021/ma2014029 |Macromolecules 2011, 44, 9399–9410

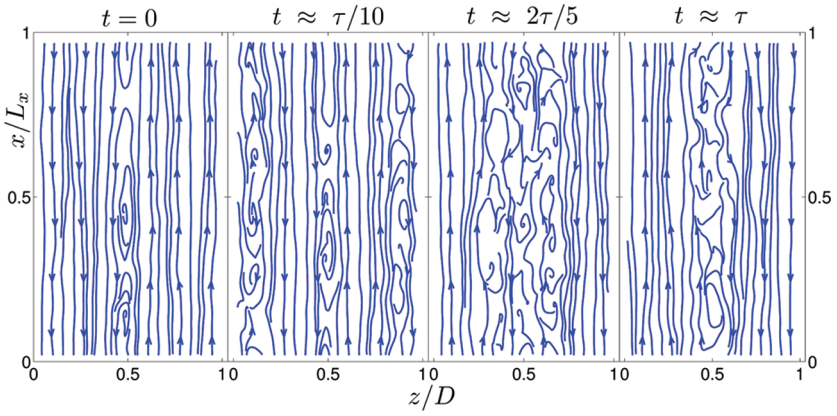

Figure 15. Flowprofiles of the dimeric solvent in steady state ($t = 0$), shortly after the inversion ($t \approx \tau/10$ and $t \approx 2\tau/5$), and at the characteristic time ($t \approx \tau$) for system B with $N = 30$, $\rho_g/\rho_g^* \approx 2.2$, $\dot{\gamma} = 0.026$. In steady state, we observe microeddies in the center. Shortly after the inversion, additional eddies appear close to the substrates, which propagate toward the center with increasing time. Already at $t \approx \tau$, the eddies are strongly reduced.

two peaks at positions, where brushes and dimers are at rest. At $t \approx \tau$, we again observe that the velocity profiles of brushes and dimeric solvent coincide, but now the presence of the colloidal inclusions destroys the linearity of the profiles. Note that monomers of colloids display a velocity profile close to those of brushes and dimers. As for system B, we observe the almost stationary profiles of the inverted steady state at $t \approx 4\tau$.

Figure 15 displays flow profiles of the dimeric solvent (system B) in the xz-plane at steady state and during shear inversion. At steady state ($t = 0$), the solvent flow is almost laminar, apart from small eddies in the center, which presumably occur due to the cyclic motion of the chain ends and the concomitant inversion of the solvent's flow direction that has been reported earlier.[31] At $t \approx \tau/10$, we observe microeddies appearing close to the substrates, which gradually propagate toward the center of the bilayer, leading to strong deviations from the laminar flow profile at $t \approx 2\tau/5$. We speculate that the eddies are a direct consequence of the finite inertia of the solvent, which appears to be of importance when the direction of shear is inverted, in particular at large Weissenberg numbers. Close to the characteristic time ($t \approx \tau$) the eddies are strongly diminished.

Systems with colloidal inclusions (not shown) exhibit similar properties when sufficient dimeric solvent is included. However, as we have seen in Figure 14, the colloids themselves perform a rotational motion during steady shear. In principle, the inclusions lead to similar effects as the dimers when the shear direction is inverted; the colloids have to invert their direction of rotation and overcome the corresponding inertia. As we will see in the upcoming section, both rotational motion of the inclusions as well as the occurrence of microeddies seem to influence the collective response of the bilayer in gradient direction.

D. Collective Response in the Gradient Direction. We now focus on the normal force necessary to keep the bilayer at a given distance. As we have seen in Figure 4d, we observe an almost constant value of f_z during steady state, i.e., the normal force virtually does not depend on the shear rate. It has been reported that f_z increases during oscillatory motion. A sudden increase of normal forces was found in experiments[3,7,8] for oscillatory shear motion. In principle, this behavior could result from chain detachment or degradation, but data from Brownian dynamics simulations,[19] where such effects can be avoided, also suggest an increased normal force. However, this conclusion was criticized in a later review article by Grest,[22] because the investigated

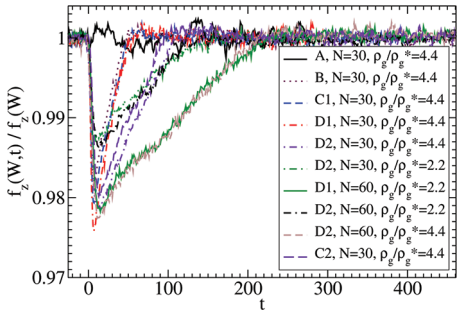

Figure 16. Time-development of the force in gradient direction, normalized by its value at steady state ($\dot{\gamma} = 0.026$). We observe a small undershoot directly after the inversion for all explicit solvents, but not for the implicit solvent (A). Beyond the minimum, the normal force increases gradually until the steady-state value establishes again.

amplitudes were only of the order of the typical distance between grafting points.

Figure 16 displays the time-development of the normal force during the inversion process. In fact, we do not find an overshoot,[63] but, in contrary, we observe an undershoot for the ratio $f_z(W,t)/f_z(W)$. The position of the minimum on the time axis is independent of the considered solvent, albeit from solvent A, where we, in agreement with an earlier study,[25] do not find any response to the shear inversion. Again, this demonstrates the importance to account explicitly for solvent molecules, in particular with respect to nonstationary processes.

A possible explanation for the occurrence of an undershoot may be related to the inertia of the solvent and the concomitant development of microeddies during the inversion process, which we have observed in section IV.C. As it seems, these eddies and, in case of embedded colloids, the rotational motion of the inclusions, invoke a force in gradient direction, which pulls on the grafted chains, leading to a decreasing normal force at the grafting points. Note that the inertia of both dimers and colloids is not related to the molecular parameters of the bilayer. Therefore, the short-time response of $f_z(W,t)$ does not display a specific characteristic time dependent on N or ρ_g, as observed in Figure 16, where the minimum appears on a very short time scale, practically independent of the molecular parameters.

dx.doi.org/10.1021/ma2014029 |Macromolecules 2011, 44, 9399–9410

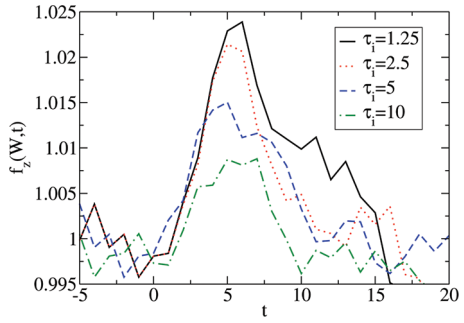

Figure 17. Overshoot of the force in gradient direction immediately after the inversion for system B with $N = 30$, $\rho_g/\rho_g^* \approx 2.2$, $\dot{\gamma} = 0.026$ using various "turn-times", τ_i. The overshoot disappears for values of $\tau_i \geq 15$. We do not observe an overshoot for any other system under consideration.

After the minimum is reached, $f_z(W,t)$ goes back to the steady-state value on a significantly larger time scale. Note that this time scale is smaller than the time needed to reestablish the shear force, in particular for solvent B, where we observe the overshoot in $f_x(W,t)$. It is difficult to speculate how the second process beyond the minimum comes about. For instance, we can exclude that a simple diffusion of the solvent, which has to flow back into the brushes and leave them again, dominates this process, because the related time scale should again not show a (clear) dependence on the molecular parameters. Since we observe such a dependence, we may conclude that a more complex scenario, which also involves a relaxation of the chains, is responsible for our observations.

Remarkably, our data indicate that the undershoot can be as pronounced for systems with colloidal inclusions as for the simple solvent B. Concerning the normal force, colloidal inclusions seem not to reveal any favorable features, which may appear as a contradiction to our conclusions drawn from the shear force. In fact, the time window, in which the instability occurs, is smaller for the normal force as compared to the shear force and the effect as well is weaker. Moreover, a decrease of forces in gradient direction is not necessarily unfavorable. As long as the distance between the surfaces remains constant, e.g., due to external constraining forces, we still can conclude that colloidal inclusions stabilize the nonstationary process, at least for the parameters considered here. It remains to future work to identify the ideal configuration with respect to molecular parameters, density, and structure of the embedded material, which provides the best lubrication properties for both stationary and nonstationary shear.

E. Influence of the Turn-Time. Up to now, we did not discuss the influence of the turn-time, τ_i, on our results. As already mentioned, we need τ_i to be significantly smaller than the largest relaxation time of the bilayer, i.e. $\tau_i \ll \tau_b$, in order to reproduce a highly nonstationary process as it occurs in LAOS experiments. On the other hand, we must not choose τ_i too small, such that the resulting accelerations remain finite. In fact, setting τ_i to zero leads to artifacts, such as a large overshoot in the normal force, and we would not reproduce the experimental situation correctly. The question that remains so far concerns the "optimal" choice of τ_i.

In order to get an impression of the influence of the turn-time on our results we tried out several values of τ_i. While a variation of τ_i has little impact on the shear force or the conformational response, Figure 17 shows that, for small values of τ_i, the normal force exhibits an overshoot just after the inversion. This overshoot is only found for solvent B. Again, one could speculate that solvent A does not reproduce this overshoot because it is too close to the linear regime or lacks the necessary incompressibility, while the colloids smooth the instabilities. However, increasing the turn-time leads to a decrease of the overshoot, which disappears for values above $\tau_i \approx 15$. We used the latter value for the data presented above, such that no overshoot in f_z appears, while we still fulfill the constraint that $\tau_i \ll \tau_b$.

V. CONCLUSIONS

In the present article, we have shown, using molecular dynamics simulations, that our recently developed scaling theory,[33] which describes the response of strongly compressed, semidilute polymer-brush bilayers to stationary shear, can be extended to bilayers that contain colloidal inclusions and, more importantly, to nonstationary processes, as the quasi-instantaneous inversion of the shear direction. Shortly after the inversion, the overlap between the two opposing brushes increases, which can provoke mechanical instabilities, e.g., an overshoot of the shear force, as it is also observed experimentally.[8] The time, at which the overlap reaches a maximum, determines a characteristic time scale, allowing to build up a scaling argument to characterize the response of the bilayer shortly after the inversion. This approach leads to scaling plots for conformational and collective quantities, which are capable of describing our numerical data, at least on short time scales. The characteristic time can be expressed in terms of the molecular parameters of the brushes, their distance, and the shear rate, such that

$$\tau \sim \frac{N}{D\dot{\gamma}^{0.73}} \tag{30}$$

where (almost) no dependence on the grafting density is found. Note that the prefactors, effective monomer size and viscosity of the solvent, which are set to unity in eq 30, depend on the composition of the system and therefore indirectly on the molecular parameters of brushes and colloids.

We observe that bilayers with a simple (dimeric) solvent reveal an overshoot of the shear force. This effect is not reproduced by an approach with an implicit solvent, which means that previous simulations, where no explicit solvent was included, should be critically reviewed. Despite that colloidal inclusions increase the kinetic friction coefficient in steady-state shear motion, we could demonstrate that such inclusions can diminish or even suppress the overshoot after shear inversion. This effect should be of particular importance in biological systems, where innumerous inversion processes take place practically without the occurrence of wear. We believe that this is important for the lubrication in synovial joints and can also be relevant for technical applications, e.g., in artificial joints.

Analyzing density profiles of brushes, solvent, and colloids we find that solvent is expelled from the brushes into the interpenetration zone in steady state, while it tends to flow back into the brushes during shear inversion. The effect is much weaker for systems with colloidal inclusions as compared to pure brushes[33] and is also visible for the colloidal inclusions themselves. Within a certain time window during the inversion, the grafted chains do not feel their connectivity, which leads to a linear velocity profile that cannot be distinguished from that of the simple solvent. Instead of performing a translational motion, colloidal inclusions tend to rotate in steady state. When the shear direction is inverted, this rotation invokes strong inertia effects.

Consequently, we observe a small decrease of the normal force shortly after the inversion, both for systems with a purely dimeric solvent and for systems with colloidal inclusions. Also here, the implicit solvent approach fails to reproduce the effect. Since the time scale, on which we observe the decrease of the normal force, seems not to depend on the molecular parameters and is absent without an explicit solvent, we may speculate that the effect stems from the inertia, related to the occurrence of microeddies during the backflow of the solvent and, for colloidal inclusions, the rotational motion.

Our observation of the decreasing force in gradient direction, in particular the absence of an overshoot, is in marked contrast to the experimental observation.[3,7,8] When the experiment is done under perfect control of the bilayer before and after shearing, degradation and chain detachment may be excluded as a source of this discrepancy. However, to date, experiments cannot monitor molecular details during (non)stationary shear motion, such that effects like chain detachment and later reattachment or degradation of chain segments followed by recombination with other chains might still play a role. On the other hand, it can very well be that the chain lengths considered here, which are orders of magnitude smaller than in the experiment, are too small to reproduce the overshoot. In general, the origin of the mismatch between experimental and numerical results remains unclear.

Despite that the present study might be regarded as an important step toward a more realistic description of biological systems than the typically investigated case of pure brushes, many features that may be relevant for biomechanical transport processes are still not included. For instance, biopolymers are heteropolymers and typically carry an electrical charge. In addition, other structures of the embedded material, e.g., bottle-brushes, shall be considered in future work.

■ ACKNOWLEDGMENT

We thank J. Baschnagel, K. Binder, A. Johner, and J.-U. Sommer for helpful discussions. Furthermore, we acknowledge financial support by a stipend of the "Exzellenzinitiative des Bundes und der Länder", the Agence Nationale de la Recherche (ANR-06-BLAN-0315), and the MENESR. T.K. and L.S. thank the Institute of Physics at the University of Mainz and the Institut Charles Sadron for hospitality during several short visits and the European Science Foundation for funding.

■ REFERENCES

(1) Advincula, R. C., Brittain, W. J., Caster, K. C., Rühe, J., Eds. *Polymer Brushes*; Wiley-VCH: Weinheim, Germany, 2004.
(2) Klein, J.; Perahia, D.; Warburg, S. *Nature* **1991**, *352*, 143.
(3) Klein, J. *Annu. Rev. Mater. Sci.* **1996**, *26*, 581.
(4) Schorr, P. A.; Kwan, T. C. B.; Kilbey, S. M., II; Shaqfey, E. S. G.; Tirrell, M. *Macromolecules* **2003**, *36*, 389.
(5) Tadmor, R.; Janik, J.; Klein, J.; Fetters, L. J. *Phys. Rev. Lett.* **2003**, *91*, 115503.
(6) Müller, M. T.; Yan, X.; Lee, S.; Perry, S. S.; Spencer, N. D. *Macromolecules* **2005**, *38*, 5706.
(7) Eiser, E.; Klein, J. *Macromolecules* **2007**, *40*, 8455.
(8) Klein, J. *Proc. IMechE J* **2006**, *220*, 691. *Science* **2009**, *323*, 47.
(9) Drobek, T.; Spencer, N. D. *Langmuir* **2008**, *24*, 1484.
(10) Brady, M. A.; Limpoco, F. T.; Perry, S. S. *Langmuir* **2009**, *25*, 7443.
(11) Vyas, M. K.; Nandan, B.; Schneider, K.; Stamm, M. *Eur. Polym. J.* **2009**, *45*, 1367.
(12) Zhang, Z.; Morse, A. J.; Armes, S. P.; Lewis, A. L.; Geoghegan, M.; Leggett, G. J. *Langmuir* **2011**, *27*, 2514.
(13) Murat, M.; Grest, G. S. *Phys. Rev. Lett.* **1989**, *63*, 1074.
(14) Grest, G. S.; Murat, M. *Macromolecules* **1993**, *26*, 3108.
(15) Lai, P.-Y.; Binder, K. *J. Chem. Phys.* **1993**, *98*, 2366.
(16) Miao, L.; Hong, G.; Zuckermann, M. J. *Macromolecules* **1996**, *29*, 2289.
(17) Lai, P.-Y.; Lai, C.-Y. *Phys. Rev. E* **1996**, *54*, 6958.
(18) Grest, G. S. *Phys. Rev. Lett.* **1997**, *76*, 4979.
(19) Doyle, P. S.; Shaqfeh, E. S. G.; Gast, A. P. *Phys. Rev. Lett.* **1997**, *78*, 1182. *Macromolecules* **1998**, *31*, 5474.
(20) Saphiannikova, M. G.; Pryamitsyn, V. A.; Cosgrove, T. *Macromolecules* **1998**, *31*, 6662.
(21) Neelov, I. M.; Borisov, O. V.; Binder, K. *Macromol. Theory Simul.* **1998**, *7*, 141.
(22) Grest, G. S.; Granick, S. *Adv. Polym. Sci.* **1999**, *138*, 149.
(23) Kreer, T.; Müser, M. H.; Binder, K.; Klein, J. *Langmuir* **2001**, *17*, 7804.
(24) Irfachsyad, D.; Tildesley, D.; Malfreyt, P. *Phys. Chem. Chem. Phys.* **2002**, *4*, 3008.
(25) Kreer, T.; Binder, K.; Müser, M. H. *Langmuir* **2003**, *19*, 7551.
(26) Kreer, T.; Müser, M. H. *Wear* **2003**, *254*, 827.
(27) Goujon, F.; Malfreyt, P.; Tildesley, D. J. *ChemPhysChem* **2004**, *5*, 457. *Mol. Phys.* **2005**, *103*, 2675. *Macromolecules* **2009**, *42*, 4310. *Soft Matter* **2010**, *6*, 3472.
(28) Pastorino, C.; Binder, K.; Kreer, T.; Müller, M. *J. Chem. Phys.* **2006**, *124*, 064902.
(29) Pastorino, C.; Kreer, T.; Müller, M.; Binder, K. *Phys. Rev. E* **2007**, *76*, 026706.
(30) Dimitrov, D. I.; Milchev, A.; Binder, K. *J. Chem. Phys.* **2007**, *127*, 084905.
(31) Müller, M.; Pastorino, C. *Europhys. Lett.* **2008**, *81*, 28002.
(32) Kim, Y. W.; Lobaskin, V.; Gutsche, C.; Kremer, F.; Pincus, P.; Netz, R. R. *Macromolecules* **2009**, *42*, 3650.
(33) Galuschko, A.; Spirin, L.; Kreer, T.; Johner, A.; Pastorino, C.; Wittmer, J. P.; Baschnagel, J. *Langmuir* **2010**, *26*, 6418.
(34) Spirin, L.; Galuschko, A.; Kreer, T.; Johner, A.; Baschnagel, J.; Binder, K. *Eur. Phys. J. E* **2010**, *33*, 307.
(35) Milchev, A.; Dimitrov, D. I.; Binder, K. *Biomicrofluidics* **2010**, *4*, 032202.
(36) Cao, Q.; Zuo, C.; Li, L.; He, H. *Modelling Simul. Mater. Sci. Eng.* **2010**, *18*, 075001.
(37) Spirin, L.; Galuschko, A.; Kreer, T.; Binder, K.; Baschnagel, J. *Phys. Rev. Lett.* **2011**, *106*, 168301.
(38) Milner, S. T.; Witten, T. A.; Cates, M. E. *Macromolecules* **1988**, *21*, 2610. *Europhys. Lett.* **1988**, *5*, 413.
(39) Zhulina, E. B.; Pryamitsyn, V. A.; Borisov, O. V. *Polym. Sci. USSR* **1989**, *31*, 205.
(40) Witten, T. A.; Leibler, L.; Pincus, P. A. *Macromolecules* **1990**, *23*, 824.
(41) Joanny, J.-F. *Langmuir* **1992**, *8*, 989.
(42) Netz, R. R.; Schick, M. *Europhys. Lett.* **1997**, *38*, 37.
(43) Clement, F.; Charitat, T.; Johner, A.; Joanny, J.-F. *Europhys. Lett.* **2001**, *54*, 65.
(44) Sendner, C.; Netz, R. R. *Eur. Phys. J. E* **2009**, *30*, 75.
(45) Huang, C.-C.; Winkler, R. G.; Sutmann, G.; Gompper, G. *Macromolecules* **2010**, *43*, 10107.
(46) Philippoff, W. *Trans. Soc. Rheol.* **1966**, *10*, 317.
(47) Grest, G. S.; Kremer, K. *Phys. Rev. A* **1986**, *33*, 3628. Kremer, K.; Grest, G. S. *J. Chem. Phys.* **1990**, *92*, 5057.
(48) Meyer, H.; Kreer, T.; Cavallo, A.; Wittmer, J. P.; Baschnagel, J. *Eur. Phys. J. - Special Topics* **2007**, *141*, 167.
(49) For convenience, we express the grafting density for $N = 60$ in terms of ρ_g^* for $N = 30$.
(50) Note that this value of R_g corresponds to the extension of a single chain *without* an explicit solvent. With the explicit solvents of our models R_g should be different. The value given for ρ_g^* is a rough estimate for the critical grafting density.

(51) Since the LJ interaction between the monomers is always repulsive, good solvent conditions establish even for the implicit solvent.
(52) Frenkel, D.; Smit, B., *Understanding Molecular Simulation*, 2nd ed.; Academic Press: San Diego, CA, 2002.
(53) Hoogerbrugge, P. J.; Koelman, J. M. V. A. *Europhys. Lett.* **1992**, *19*, 155.
(54) Espanol, P. *Phys. Rev. E* **1995**, *52*, 1734.
(55) Espanol, P.; Warren, P. *Europhys. Lett.* **1995**, *30*, 191.
(56) Groot, R. D.; Warren, P. B. *J. Chem. Phys.* **1997**, *107*, 4423.
(57) P. G. de Gennes, *Scaling Concepts in Polymer Physics*; Cornell University Press: New York, 1979.
(58) Here and in the following, we present all quantities in LJ units.
(59) Dünweg, B.; Kremer, K. *Phys. Rev. Lett.* **1991**, *66*, 2996.
(60) J. Des Cloizeaux, Jannik, G., *Polymers in Solution*; Oxford University Press: Oxford, U.K., 2010).
(61) Schäfer, L., *Excluded Volume Effects in Polymer Solutions*; Springer: Berlin, 1999).
(62) In principle, one could determine a and η_s from independent simulations in steady state, measuring e.g. the mobility of monomers or the relaxation time of the bilayer (as done in ref 33) and compare to eq 16.
(63) As we will see in section IV.E, this statement is only valid if the "turn-time" is chosen to be large enough.